Carbon 158 (2020) 426–434

Contents lists available at ScienceDirect

Carbon

journal homepage: www.elsevier.com/locate/carbon

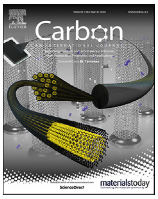

Ultra-stiff graphene oxide paper prepared by directed-flow vacuum filtration

Siyu Liu [a], Kaiwen Hu [b], Marta Cerruti [c], Francois Barthelat [a, d, *]

[a] *Department of Mechanical Engineering, McGill University, 817 Sherbrooke Street West, Montreal, QC H3A 2K6, Canada*
[b] *Department of Electrical and Computer Engineering, McGill University, 817 Sherbrooke Street West, Montreal, QC, H3A 2A7, Canada*
[c] *Department of Mining and Materials Engineering, McGill University, 817 Sherbrooke Street West, Montreal, QC, H3A 0C5, Canada*
[d] *Department of Mechanical Engineering, University of Colorado, 427 UCB, 1111 Engineering Dr, Boulder, CO, 80309, USA*

ARTICLE INFO

Article history:
Received 8 June 2019
Received in revised form
31 October 2019
Accepted 3 November 2019
Available online 12 November 2019

ABSTRACT

Graphene oxide (GO) paper is an attracting structural material because of its high stiffness and lightweight. In order to exploit the high strength and stiffness of individual GO nanosheet into GO paper, the fabrication process must be optimized. In this study we fabricated ultra-stiff and strong GO paper by directed-flow vacuum filtration and compared its mechanical properties under different loading conditions. We also explored the effect of cross-linking with borax, thermal annealing and sonication to further enhance mechanical properties. The stiffest GO paper reported here has a tensile modulus of 109.9 GPa and a flexural modulus of 45.7 GPa. We also found that the flexural modulus of GO paper is significantly lower than the tensile modulus because of interlayer shearing, micro-buckling and delamination during flexural deformation. The properties of GO papers therefore need to be carefully selected for mechanical structures where flexion is the major deformation. This study provides significant insights about improving mechanical properties of GO paper and selecting GO paper for different loading conditions.

1. Introduction

Free-standing paper-like materials assembled from graphene-based nanosheets have been receiving great attention from researchers because of their extraordinary mechanical and electrical properties. Graphene and graphene oxide (GO) membranes have achieved broad applications including microphones [1,2], earphones [3], humidity sensors [4], electromechanical resonators [5], molecular sieving [6], and protective barriers [7]. GO includes several oxygen-containing functional groups (mainly hydroxyl, carboxyl, carbonyl and epoxide) as defects in an sp^2-bonded graphene carbon structure [8]. Individual GO nanosheets can be assembled into GO paper using a variety of methods: directed-flow vacuum filtration [9–11], spin casting [12], spray coating [13], Langmuir-Blodgett assembly [14], and self-assembly at the liquid/air interface [15]. Among these strategies, the vacuum filtration is a relatively simple and scalable method which produces a layered structure in which individual GO sheets are interlocked or tiled in a near-parallel direction [9]. Monolayer GO has a Young's modulus of 207.6 GPa obtained by atomic force microscopy [16], while its predicted fracture stress is 63 GPa from molecular dynamics simulations [17]. However, when individual monolayers are assembled into mesoscopic sheets or "paper", these mechanical properties decrease significantly because GO sheets are only weakly connected by hydrogen bonds and van der Waals interactions [18]. For instance, a GO paper with a thickness of 22 μm has a Young's modulus of only 22 GPa and an ultimate strength of 39 MPa [9]. Chemical cross-linking between the oxygen-containing groups of individual GO sheets is required to increase these properties. To this day, various cross-linkers have been used to stiffen and strengthen GO paper: Mg^{2+} [19], Ca^{2+} [19], Cu^{2+} [20], PVA (poly(vinyl alcohol)) [21], PMMA (poly(methyl methacrylate)) [21], PAA (polyallylamine) [22], PEI (polyallylamine) [23], PAH (poly(allylamine) hydrochloride) [24], PCDO (10,12-pentacosadiyn-1-ol) [25], borate ions [26], dopamine [27], gellan gum [28], glutaraldehyde [29] and silk fibroin [30]. Among these cross-linkers, borate ions appear to be the most effective: the Young's modulus and the ultimate strength of GO paper after cross-linking with borate ions can be enhanced to 127 GPa and 185 MPa, respectively [26].

---

* Corresponding author. Department of Mechanical Engineering, McGill University, 817 Sherbrooke Street West, Montreal, QC H3A 2K6, Canada.
E-mail address: francois.barthelat@colorado.edu (F. Barthelat).

https://doi.org/10.1016/j.carbon.2019.11.007
0008-6223/© 2019 Published by Elsevier Ltd.

The thickness of GO paper is another critical parameter that governs its mechanical properties, thinner papers tending to have higher Young's modulus and strength than thicker ones. For example, Gong and coworkers reported a decrease of Young's modulus from 44.6 GPa to 8.5 GPa when the thickness of the paper is increased from 0.5 μm to 100 μm [31], an effect attributed to the higher number of defects in thicker papers. For this reason, most of the literature on GO paper focuses on GO papers with thickness below 30 μm. Thin GO papers are however inherently difficult to handle because they are difficult to be peeled from the substrate and can easily get broken during the transfer process. Moreover, the stiffness of a structure relates to both of the Young's modulus and the structure dimensions, so thin GO papers may have low structural stiffness because of their small thickness, limiting the range of their applications. Fabricating relatively thick GO paper while maintaining high Young's modulus and strength is still a challenge to this day. In addition, most mechanical tests reported in the GO paper literature focus on uniaxial tension, with tensile properties that may not be representative of applications that involve flexural deformations. GO paper in flexion may undergo delamination and micro-buckling, two dangerous failure modes which are not captured in tensile tests.

In this study, we fabricated GO papers with different thicknesses by directed-flow vacuum filtration, combined with additional fabrication steps: borax cross-linking, thermal annealing and sonication. The chemical properties of GO papers were characterized by Fourier Transform infrared spectroscopy (FT-IR), X-ray photoelectron spectroscopy (XPS) and thermogravimetric analysis (TGA). Mechanical properties (Young's modulus and ultimate strength) were tested by both tension and flexion. This research provides significant insights about improving mechanical properties of GO paper and selecting GO paper for different loading conditions, making this material suitable for a wider range of applications.

2. Basic fabrication protocol and characterization

2.1. Fabrication

Fabrication started by dissolving GO paste (Abalonyx Innovative Materials) in water to produce a suspension with a GO concentration of 10 mg/mL. Individual GO sheets were exfoliated and dispersed by magnetic stirring for 30 min. A controlled volume of this suspension was then poured on a hydrophilic PVDF filtrate membrane (Sigma-Aldrich, 90 mm diameter and 0.22 μm pore size) mounted on a vacuum chamber (Fig. 1a). A vacuum pump produced a −635 mm Hg vacuum that pulled water through the filter, leaving GO sheets with a well-organized order onto the filter membrane. Once the entire solution was filtrated (typically in about 24 h), a dried patch of GO paper (Fig. 1b) could be manually separated from the filter membrane. The resulting paper was flat and smooth, with a uniform thickness.

For all the study we used the same type of solution with GO concentration of 10 mg/mL, so that the thickness of the GO paper was proportional to the volume of GO solution filtrated. We prepared pure GO papers with thicknesses of 35 μm, 86 μm and 138 μm by filtering 28.5 mL, 57.0 mL and 85.5 mL of solution respectively. The GO papers were prepared and mechanically tested in an environment with a constant humidity of 30–50% and temperature of 20–25 °C (the mechanical properties of GO paper generally vary with humidity in the air because of the oxygen-containing functional groups in GO [32]).

2.2. Basic characterizations

The pure GO papers were characterized by Fourier Transform infrared spectroscopy (FT-IR using a spectrum-two IR spectrometer, PerkinElmer), X-ray photoelectron spectroscopy (XPS using a monochromatic Al Kα photoelectron spectrometer, Thermo Scientific) and thermogravimetric analysis (TGA Q500, TA instrument). The FT-IR spectrum of the pure GO (Fig. 2a) shows absorptions at corresponding $\nu_{\text{O-H}}$ (3670–2900 cm^{-1}), $\nu_{\text{C=O}}$ (1716 cm^{-1}), δ_{H2O} (1623 cm^{-1}), $\delta_{\text{O-H}}$ (1410 cm^{-1}) and $\nu_{\text{C-O}}$ (1045 cm^{-1}) [33]. No organic impurities were detected from the FT-IR spectrum. The high-resolution C1s XPS spectrum (Fig. 2b) of the pure GO reveals four components: C–C (284.8 eV), C–O (286.4 eV), C=O (288.4 eV), and π-π* shake up (290.9 eV) [34]. The atomic percentage of C–C is 54 ± 3%, which indicates the oxidation degree of the GO. Very small amount of N (1%) and Si (0.4%) were detected only on one out of three spots analyzed, indicating that the initial material was quite pure. TGA was performed under air with a temperature ramp of 15 °C/min from room temperature up to 400 °C. The TGA curve (Fig. 2c, in derivative plot) of the pure GO paper shows two main peaks corresponding to two main drops in weight: the first weight drop is caused by the evaporation of water in GO, while the second one (228 °C) is caused by the decomposition of oxygen-containing functional groups [24]. The second peak reflects the thermal stability of the GO paper. In order to characterize the sheet size of GO, the original 10 mg/mL GO suspension was diluted to 10 μg/mL and suspended on a glass plate by drop casting. The overall range of the sheet size is 1–25 μm (median value 5 μm) from the optical microscopy image (Fig. 2d), which matches the information provided by the manufacturer that the sheet size is 2–20 μm.

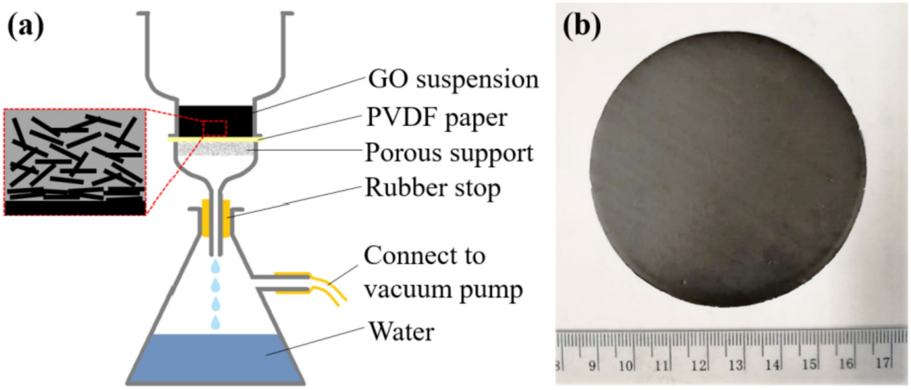

Fig. 1. Fabrication of GO paper by directed-flow vacuum filtration: (a) equipment for vacuum filtration; (b) a piece of filtrated GO paper with the thickness of 86 μm. (A colour version of this figure can be viewed online.)

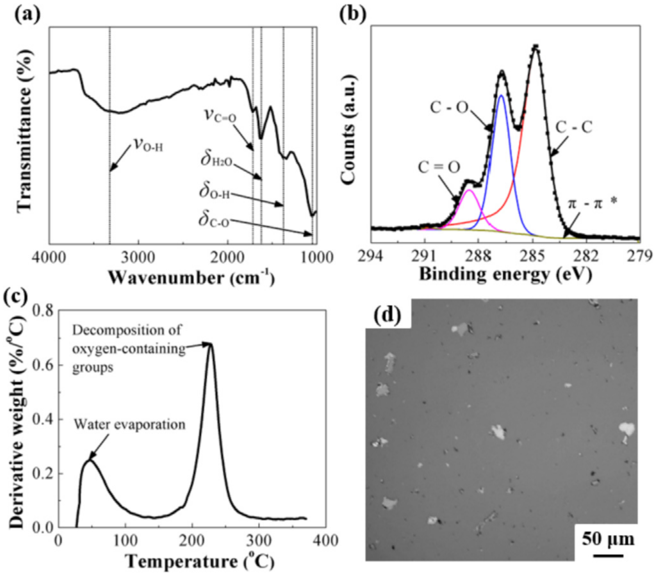

Fig. 2. Characterization of pure GO paper: (a) FT-IR spectrum; (b) deconvoluted C1s XPS spectrum: the collected spectrum is shown with black dots; the fitted components in red (C–C), blue (C–O), purple (C═O) and dark yellow (π-π* shake up), and the overall fit in black; (c) derivative TGA curve; (d) optical microscope image of the drop casted GO suspension. (A colour version of this figure can be viewed online.)

2.3. Imaging

The cross-section morphology of the GO papers obtained by vacuum filtration was characterized by scanning electron microscopy (SEM). The samples were prepared by mounting GO paper in a polymer resin (EpoThin epoxy) vertically, followed by polishing to obtain a flat and smooth cross-section of the film. The sample was polished using 6 μm, 1 μm and 0.25 μm polycrystalline diamond suspensions across the direction of the layers to minimize further damage. The sample was then coated with a 4 nm thick platinum layer (Leica ACE600 sputter coater) to prevent charging. Then the images were collected using a field emission scanning electron microscope (FEI Inspect F50 FE-SEM) with an accelerating voltage of 5 kV. SEM images (Fig. 3) revealed that thin samples are relatively dense, with few cracks and voids. Thicker samples had less regular alignment of the layers and contained long delamination cracks (Fig. 3b and c). These cracks were also observed in the cross-section before polishing. The implications of these defects on mechanical properties are explored in the next section.

2.4. Mechanical tests

The mechanical properties of the GO films were measured using flexion (three-point bending) and tension, two loading configurations which are representative of many current and possible applications for GO paper. The samples were laser-cut (Model Vitrolux, Vitro Laser Solutions UG) with a power of 354.8 mW and a wavelength of 355 nm. Laser cutting ensured precise control over sample geometry and dimensions and minimized mechanical damage or defects which would be otherwise created from mechanical cuts. Flexural samples were 20 mm × 1 mm–20 mm × 2 mm strips (Fig. 4a), and tensile samples were dog-bone shaped with a gage region of 15 mm by 2 mm (Fig. 4b).

The flexural tests were performed on a miniature loading stage (Ernest F. Fullam, Inc) equipped with a 20 g load cell. The samples were loaded at a rate of 0.02 mm/s until complete failure. Fig. 4a shows the flexural sample before and after the test. Failure was localized and relatively brittle. The flexural stress and strain were calculated by:

$$\sigma_f = \frac{3FL_s}{2bh^2} \tag{2.1}$$

$$\varepsilon_f = \frac{6Dh}{{L_s}^2} \tag{2.2}$$

where F is the force, D is the displacement, L_s is the span of the fixture, b is the width and h is the height of the sample. The flexural stress-strain curves (Fig. 4c) indicate that the flexural modulus and flexural strength are higher for thinner GO papers. The 35 μm thick samples were the strongest and they did not fracture, instead they slipped out of the fixture. The maximum plateau shown on the stress-strain curve for the 35 μm sample is an artifact due to sliding of the sample onto the flexural fixture. The 86 μm and 138 μm samples fractured and the flexural load drops to near zero after failure, but the two fragments were still connected by a few loosened layers. Considering the cross-sections shown on Fig. 3, we attributed the higher properties of the thinner samples to their higher density and their more compact layer architecture.

We also performed uniaxial tensile tests on these GO papers to compare their mechanical properties under different loading conditions. A 10 lb load cell and a loading rate of 0.002 mm/s were used for the tensile tests. The loading stage was placed under an optical microscope (BX-51 M, Olympus) equipped with a CCD camera (Retiga 2000R, Qimaging) during the tensile test. The image was maintained in focus on the sample surface and sequential pictures were taken by the microscope in regular intervals. Tensile strains were measured using digital image correlation (DIC) on digital images of the sample acquired during the test. In order to generate optical features for DIC, the surface of GO paper was sputtered with a random speckle of white dots. Typical tensile stress-strain curves are shown in Fig. 4d. The response is quasi linear with a slight softening up to sudden fracture at a tensile strain in the order of 0.1%. The tensile curves were used to determine the tensile

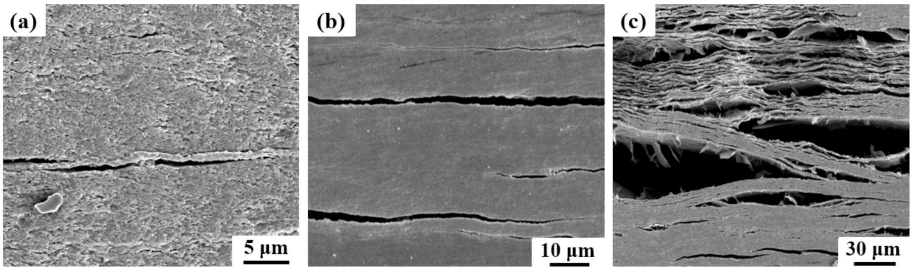

Fig. 3. Cross-section SEM of filtrated GO paper with different thicknesses: (a) 35 μm; (b) 86 μm; (c) 138 μm. (A colour version of this figure can be viewed online.)

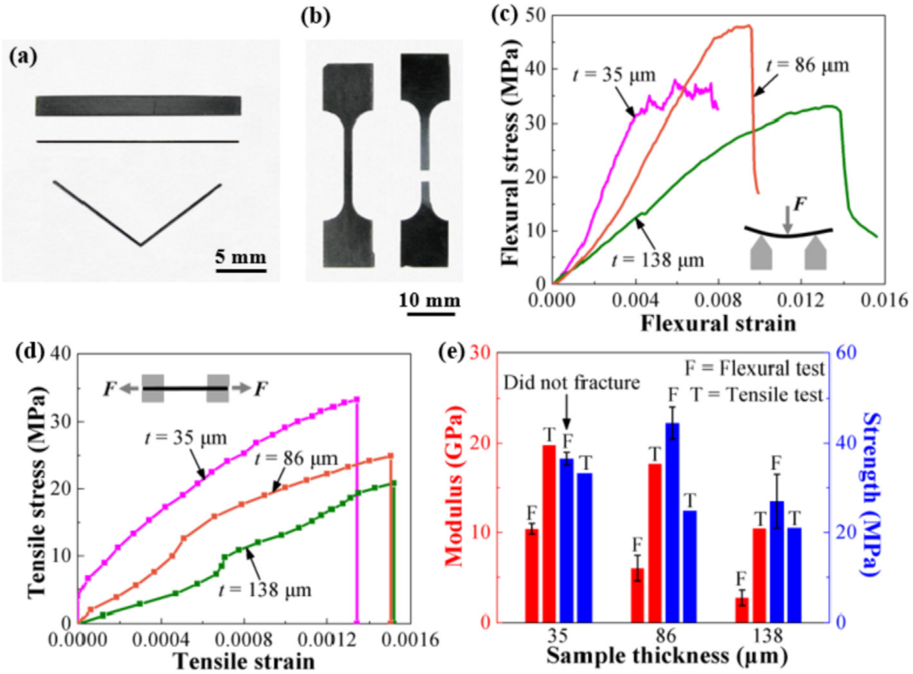

Fig. 4. Mechanical tests of GO paper with different thicknesses: (a) three-point bending specimen before (top view and side view) and after (side view) the test; (b) tensile specimen before and after the test; (c) flexural stress-strain curves; (d) tensile stress-strain curves; (e) comparison of modulus and strength for samples of various thicknesses tested in flexion and tension (the 35 μm sample did not fracture during the flexural test). (A colour version of this figure can be viewed online.)

modulus and the tensile strength for the GO paper.

Fig. 4e provides a summary of the tensile and flexural modulus and strength. The modulus is in the 3–20 GPa range, and the strength in the 20–50 MPa range. In general, both strength and modulus decrease when the thickness of the paper is increased. For the same sample, the tensile modulus is higher than the flexural modulus, while the tensile strength is lower than the flexural strength. This result indicates that the GO paper undergoes deformation mechanisms which are different in tension and flexion. More specifically, the difference of apparent mechanical properties in tension and flexion can be explained by the layered structure of the GO paper. In uniaxial tension the stress is uniform in the gage area, and every layer of the GO paper is stretched identically. In contrast, the stress in a flexural sample is tensile on one side of the sample and compressive on the other. The weak adhesion between the layers may not prevent layers on the compressive side from buckling. In this scenario the stresses carried by the buckled layers is greatly reduced (Fig. 5a) which would in turn greatly reduce the overall flexural stiffness of the material. To investigate this hypothesis, a section of GO paper (thickness = 35 μm) was mounted in a bent conformation as shown in Fig. 5b. Cross-section SEM images of this sample after polishing are shown in Fig. 5c and d. The layers remain straight and flat near the tensile face, but the compressive side shows evidence of micro-buckling of the layers. Another possible contributor to a lower flexural modulus is the shear deformation at the interfaces between the layers. The total deflection of the three-point bending test is a combination of bending and shear deformations [35]:

$$\delta_{deflection} = \frac{FL_s^3}{48E_f I} + \frac{FL_s}{4G} \tag{2.3}$$

where E_f is the flexural modulus, I is the moment of inertia and G is the shear modulus. When homogenous beams of high aspect ratio are tested in flexure, the second term can be neglected. However, this may not be possible for the GO paper if the interfaces between the layers may are very compliant ($G \ll E_f$). In this case the second term may contribute to the total deformation by a significant amount, which in effect would reduce the overall stiffness of the beam. Micro-buckling, delamination and interlayer shear deformations can therefore explain the low flexural modulus of GO paper compared to the tensile modulus.

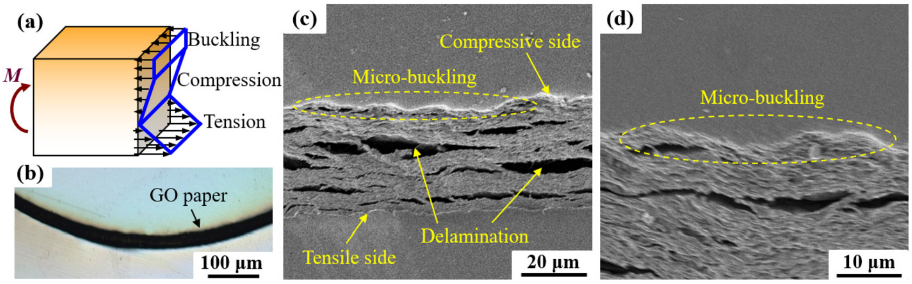

Fig. 5. Microstructure and stress condition of GO paper after flexural deformation: (a) schematic figure of normal stress condition; (b) optical microscope image of the mounted GO paper; (c) (d) cross-section SEM images of GO paper after flexural deformation. (A colour version of this figure can be viewed online.)

Despite a lower apparent stiffness in flexion, the flexural strength of the GO paper was higher than the tensile strength. We explained this difference by the presence of defects and with arguments based on weakest link statistics. For a tensile sample, the entire volume of the sample is stressed by the same amount, so that any large defect in the sample can be activated and lead to fracture. In contrast, in the three-point bending configuration, only a small fraction of the beam is loaded near the highest tensile stresses, so statistically chances to activate a large defect with these high stresses are lower than in tension. The average stress is smaller and fewer defects are involved for the flexural test, which makes GO paper stronger under flexion than tension. The differences in micromechanics between flexion and tension should be considered when applications are sought for GO paper. We used this first set of experiments as a reference for the mechanical properties of GO paper and in the next sections, we explored various steps and extra protocol to improve these properties.

3. Optimization

3.1. Cross-linking

To improve the properties of the GO paper, we first cross-linked it with borate ions. A borax solution (0.1 mol/L) was prepared by dissolving borax ($Na_2B_4O_7 \cdot 10H_2O$) powder (Sigma-Aldrich) in water using magnetic stirring at 70 °C for 30 min. 57.0 mL of GO suspension was mixed with 6.3 mL, 14.3 mL and 24.4 mL of borax solution, respectively, and the corresponding borax concentration was diluted to 0.01 mol/L, 0.02 mol/L and 0.03 mol/L after mixing. The corresponding paper thickness after filtration was 85 μm, 88 μm and 89 μm, respectively. Fig. 6 illustrates the mechanism of borax cross-linking: borax ions can form covalent borate orthoester bonds with hydroxyl and epoxide functional groups present on GO [26], while pure GO sheets are weakly connected by hydrogen bonds [18]. This mechanism is different from the cross-linking at edges through carboxyl groups that happens with divalent metal cations [19]. After borax cross-linking, the combined covalent and hydrogen bonding system stiffens the interface between the GO sheets.

The chemical properties of borax cross-linked GO papers were characterized by FT-IR and XPS. Compared to pure GO paper, the $\delta_{O\text{-}H}$ (1410 cm^{-1}) absorption band on the FT-IR spectra (Fig. 7a), is stronger and shifted to lower wavenumbers. This is due to the reversible epoxide ring opening at a higher pH caused by borax addition [36]: indeed, the addition of borax solution increased the pH of the GO suspension because of the hydrolysis of borate ions, going from 1.68 ± 0.03 for pure GO to 8.06 ± 0.16 and 8.84 ± 0.14 for 0.01 mol/L and 0.03 mol/L borax cross-linked GO suspensions, respectively (Fig. 7b). The other characteristic absorption bands have no evident shift after borax cross-linking. The deconvoluted high-resolution C1s XPS spectra of 0.01 mol/L and 0.03 mol/L borax cross-linked GO are shown in Fig. 7c and d. The atomic percentage of C—C is 58 ± 1% for the 0.01 mol/L cross-linked GO and 51 ± 4% for the 0.03 mol/L cross-linked GO, which are not significantly different than the pure GO (54 ± 3%). The detection of a clear B1s peak in XPS high-resolution spectra (Fig. 7e) indicates the presence of borax in GO paper after cross-linking. The atomic percentage of B1s is 2.1 ± 0.2% for the 0.01 mol/L cross-linked GO, and 8.4 ± 0.2% for the 0.03 mol/L cross-linked GO. The thermal stability of borax cross-linked GO papers was characterized by TGA. The TGA curves (Fig. 7f, in derivative plots) show that the weight loss peak caused by the decomposition of oxygen containing groups shifts to a lower temperature with increasing borax amount: the first evident weight loss peak (caused by decomposed oxygen-containing groups) is found at 228 °C, 222 °C and 199 °C for pure GO, 0.01 mol/L borax cross-linked GO and 0.03 mol/L borax cross-linked GO, respectively. This shift is due to the fact that GO becomes more thermally unstable when in basic pH [38].

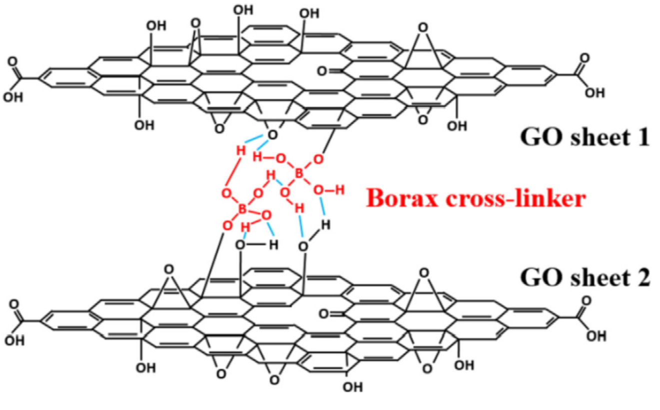

Fig. 6. Schematic figure of two adjacent GO sheets cross-linked by borax (the GO sheet structure is adapted from Ref. [37]).

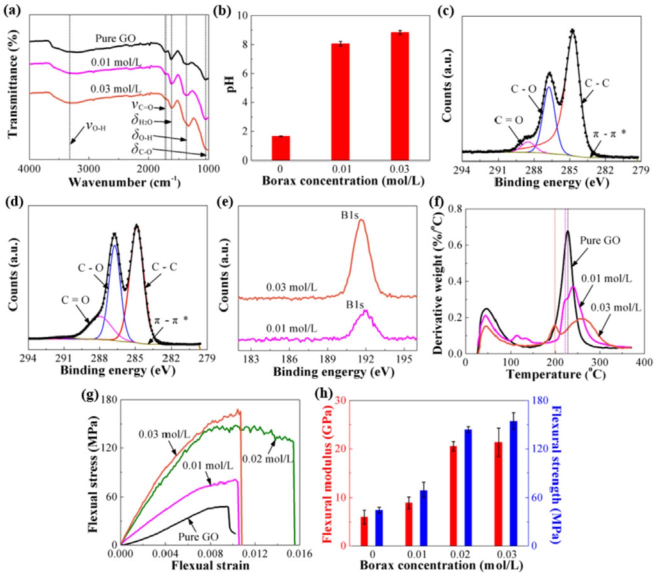

Fig. 7. Chemical and mechanical properties of borax cross-linked of GO papers: (a) FT-IR spectra of pure GO and GO cross-linked with borax; (b) pH of raw suspensions; (c) deconvoluted C1s XPS spectrum of the 0.01 mol/L borax cross-linked GO: the collected spectrum is shown with black dots; the fitted components in red (C—C), blue (C—O), purple (C═O) and dark yellow (π-π* shake up), and the overall fit in black; (d) deconvoluted C1s XPS spectrum of the 0.03 mol/L borax cross-linked GO; (e) B1s XPS spectra; (f) derivative TGA curves of GO paper and GO paper cross-linked with borax; (g) flexural stress-strain curves; (h) flexural modulus and flexural strength. (A colour version of this figure can be viewed online.)

Fig. 7g shows the flexural stress-strain curves for the pure GO paper and for GO papers with different levels of borax cross-linker. The flexural ductility of the paper had no evident changes, but the flexural modulus and the ultimate flexural strength increased significantly with higher borax concentrations (Fig. 7h). The flexural modulus of the 0.03 mol/L cross-linked GO paper is 3.55 times that of the pure sample, and the ultimate flexural strength is 3.47 times that of the pure sample. However, mechanical properties were no longer improved evidently beyond a cross-linker concentration of 0.02 mol/L. Visible aggregations were observed during filtration for very high borax concentrations because of the instability of the mixed suspension. Filtrated GO papers containing large borax concentrations have large vacancies and disordered structures and decreased mechanical properties [26].

3.2. Annealing

As another step to improve the quality of the GO paper we used thermal annealing, with the objective to reduce water content and to make the layers within the paper more compact. This process was undertaken by heating GO paper in a closed oven (Sheldon Manufacturing, Inc, Model No.1410 M), and the sample was cooled in air after heating. We firstly characterized the annealed pure GO papers by FT-IR and XPS. No evident shifts of characteristic absorption bands were observed from the FT-IR spectra (Fig. 8a). Also there were no large changes in C/O ratio in the XPS surveys (Fig. 8b) (from 1.84 ± 0.02 to 1.98 ± 0.04 after annealing, which likely reflect water evaporation) and C−C content (55 ± 6% after annealing, see Fig. 8c). These results indicate that the GO paper was not reduced during annealing. Fig. 8d shows typical flexural test results of the 86 μm pure GO paper after annealing at different temperatures. The flexural modulus increases when the annealing temperature was increased up 150 °C. The flexural modulus after annealing at 150 °C was nearly twice that of the as-prepared sample. The improved mechanical properties are caused by the evaporation of interlayer water molecules, which allows GO sheets pack tighter to enhance interlayer contacts and interactions. This was confirmed by Andrikopoulos and coworkers, who showed that the spacing between GO sheets reduces from 7.4 Å to 6.13 Å after heating at 160 °C [39]. However annealing at 200 °C led to poor mechanical properties. This is likely due to the degradation of the GO paper at this temperature, as shown by the approximately 50% decrease in sample thickness (from 86 μm to 47 μm), which damages the mechanical integrity. Fig. 8e shows the effect of annealing duration on flexural stress and modulus. The flexural modulus was higher for longer annealing times up to 120 min after which the modulus ceased to increase, while the flexural strength showed no evident increase after annealing for 40 min. We therefore used an annealing time of 120 min for the rest of this study. In summary (Fig. 8f), we found that the annealing parameters that produced the highest properties in pure GO paper are a temperature of 150 °C for 120 min.

Annealing can also be combined with borax cross-linking to further improve mechanical properties. We chose annealing temperatures of 100 °C and 150 °C, and an annealing time of 2 h for cross-linked samples. Fig. 9a and b shows the FT-IR spectra and the deconvoluted C1s XPS spectrum of the 0.03 mol/L borax cross-linked GO paper. Similar to the pure GO paper, the borax cross-linked GO paper was not partially reduced when the annealing temperature was lower than 150 °C. Three-point bending results of annealed cross-linked GO papers are shown in Fig. 9c-f: the average flexural modulus of the pure GO paper and the cross-linked GO paper with a low borax concentration can be improved slightly by increasing the annealing temperature. However the GO paper with higher borax concentrations showed a slight decreasing trend of flexural modulus at higher temperatures. This may be due to the decrease in thermal stability caused by the addition of borax (Fig. 7f).

3.3. Improved infusion protocol for the cross-linker

The borax cross-linked GO papers above were synthesized by mixing GO and borax solutions together before filtration. During this procedure only a small amount of borax remains in the filtered GO paper. To improve over this and maximize borax cross-linking, we developed a new fabrication process (Fig. 10a). In the new procedure a borax-free GO suspension was filtrated for 24 h to form a pure GO paper. A borax solution (0.02 mol/L after mixing) was then added onto the already formed GO paper for a second filtration step. Because of the presence of the GO paper on the filter, the porosity was decreased and this second filtration process was slower (48 h). Finally, the prepared GO paper was annealed at 100 °C for 2 h. GO papers with two thicknesses (39 μm and 91 μm) were synthesized by this improved procedure, and their mechanical properties are shown in Fig. 10b–d. The flexural modulus of the 91 μm sample was 18.7% higher than the sample prepared using the previous cross-linking method (in Fig. 9d, thickness 88 μm). For the 39 μm sample, the flexural modulus is 45.7 GPa and the tensile modulus is 109.9 GPa, which are the highest modulus among our GO papers. We explain these increased mechanical properties by the slower second filtration process, which allowed for an enhanced infusion of the borax cross-linker into the GO paper and

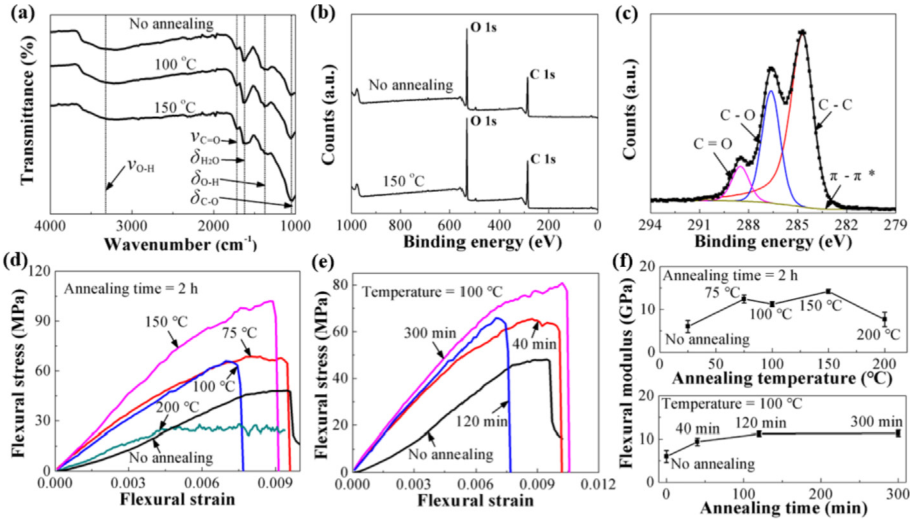

Fig. 8. Chemical and mechanical properties of annealed pure GO papers: (a) FT-IR spectra with different annealing temperatures; (b) whole survey XPS spectrum before and after annealing at 150 °C; (c) deconvoluted C1s XPS spectrum after annealing at 150 °C: the collected spectrum is shown with black dots; the fitted components in red (C−C), blue (C−O), purple (C=O) and dark yellow (π-π* shake up), and the overall fit in black; (d) flexural stress-strain curves with different annealing temperatures; (e) flexural stress-strain curves with different annealing times; (f) flexural modulus with different annealing temperatures and times. (A colour version of this figure can be viewed online.)

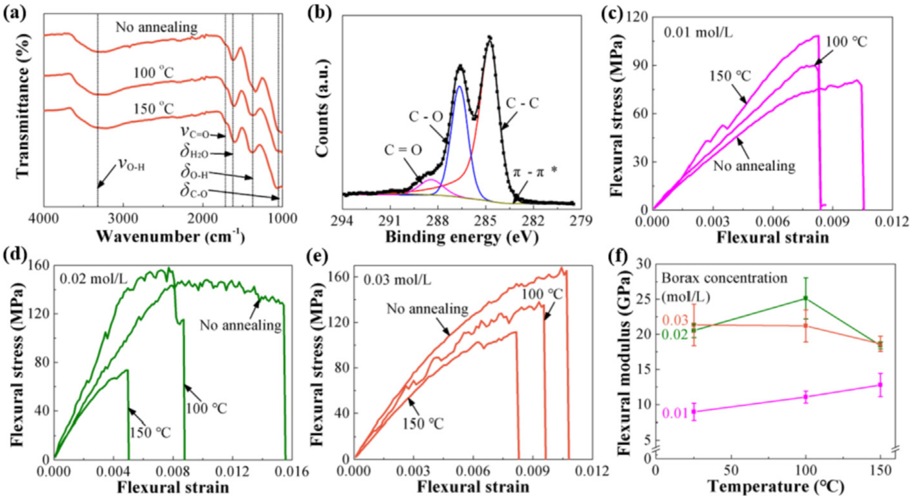

Fig. 9. Chemical and mechanical properties of annealed cross-linked GO papers: (a) FT-IR spectra of the 0.03 mol/L cross-linked GO paper with different annealing temperatures; (b) deconvoluted C1s XPS spectrum of the 0.03 mol/L cross-linked GO paper after annealing at 150 °C: the collected spectrum is shown with black dots; the fitted components in red (C–C), blue (C–O), purple (C=O) and dark yellow (π-π* shake up), and the overall fit in black; (c) flexural stress-strain curves of the 0.01 mol/L cross-linked GO paper; (d) flexural stress-strain curves of the 0.02 mol/L cross-linked GO paper; (e) flexural stress-strain curves of the 0.03 mol/L cross-linked GO paper; (f) comparison of flexural modulus. (A colour version of this figure can be viewed online.)

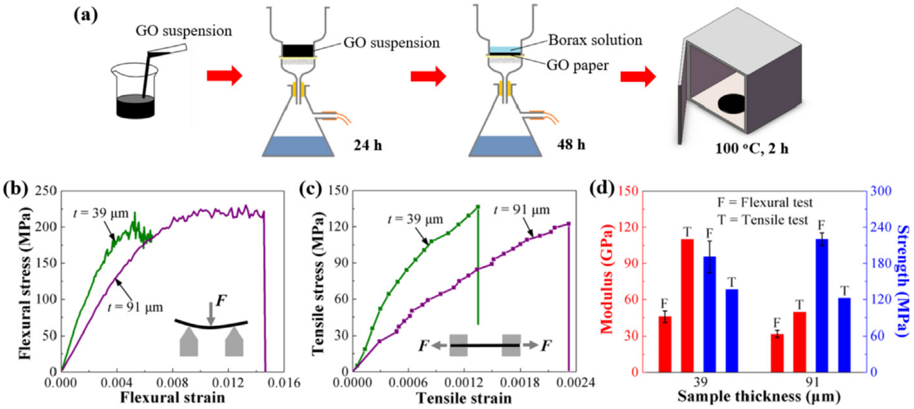

Fig. 10. Fabrication of GO paper by the improved borax cross-linking method: (a) schematic fabrication process; (b) flexural stress-strain curves; (c) tensile stress-strain curves; (d) modulus and strength of different samples. (A colour version of this figure can be viewed online.)

increased interactions of the borate ions with the oxygen-containing groups in GO.

3.4. Sonication

Sonication of GO suspension before filtration was also used with the objective to disperse the GO nanosheets more uniformly in water, and to avoid aggregation. The improved fabrication process combining borax cross-linking and sonication is shown in Fig. 11a: The GO suspension and the borax solution (0.02 mol/L after mixing) were first mixed in a beaker; then the mixed suspension was sonicated in a water-based sonicator (Branson 1510) for 1 h, followed by filtration of the suspension to form GO paper. A pure GO paper without adding borax was also fabricated for comparison. The GO suspension after sonication was also diluted to 10 μg/mL and drop casted on a glass plate (Fig. 11b). The overall range of the sheet size reduces from 1–25 μm (median value 5 μm) to 1–10 μm (median value 3 μm) after sonication.

We noted that the time required for full filtration increased from 24 h to 48 h to form the GO paper. This was reflected in a higher density of the GO paper made from sonication: we measured a density of 1.62 ± 0.02 g/cm^3 for samples prepared without sonication (pure GO), and 1.77 ± 0.03 g/cm^3 for similar samples prepared using a sonication step before GO filtration. The formation of more compact membranes implies that water was not able to go through them as easily during filtration, and explains the slower filtration rates observed for the sonicated GO suspensions. The formation of more compact membranes may be due to the fact that GO sheets became smaller and the size distribution was more uniform after sonication. The aspect of the surface (Fig. 11 c-e) after sonication also looked different: pure GO paper looks dark, while the sonicated sample, especially for the borax cross-linked one, looks brighter with more luster. This observation may indicate that these surfaces are less rough due to a better compaction of the GO sheets after sonication. Fig. 11f–h shows the results for the mechanical tests on sonicated samples. The sonication step improved the flexural modulus and the tensile modulus by 53.5% and 61.7%, respectively, compared to the pure GO paper in Fig. 4 (thickness = 35 μm). The improved mechanical properties are likely caused by the more compact structure after sonication. After combining borax cross-linking (thickness = 38 μm), the flexural modulus and the tensile modulus was further enhanced to 38.7 GPa

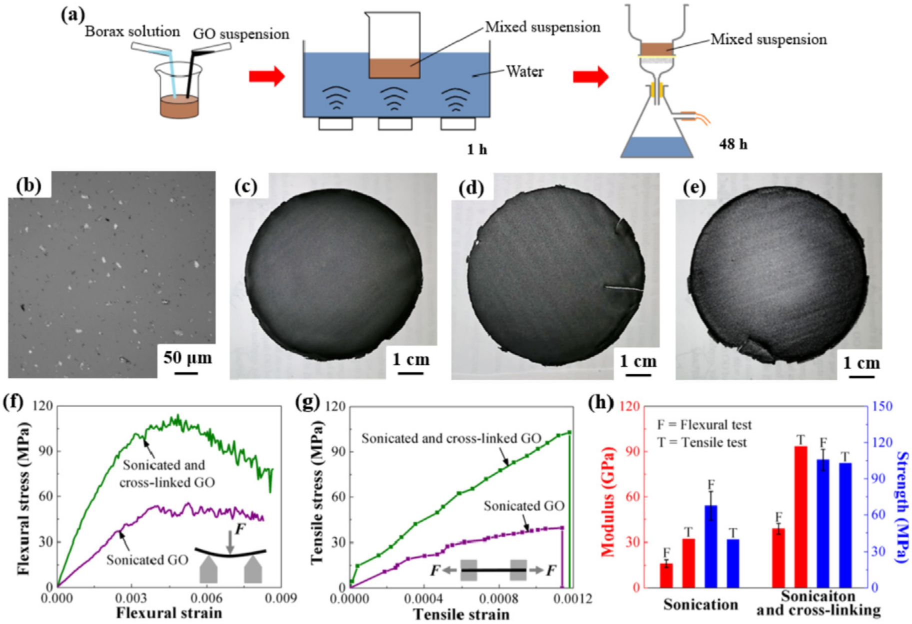

Fig. 11. Fabrication of GO paper with sonication: (a) schematic fabrication process; (b) optical microscope image of the drop casted GO suspension after sonication; (c) photograph of the pure GO paper; (d) photograph of the sonicated pure GO paper; (e) photograph of the sonicated and cross-linked GO paper; (f) flexural stress-strain curves; (g) tensile stress-strain curves; (h) modulus and strength of different samples. (A colour version of this figure can be viewed online.)

and 93.4 GPa, respectively. We were not able to fabricate thick GO papers from the sonicated solutions, due to the slow filtration rate: when we attempted to make a 90 µm GO paper the GO suspension remained in the filtration container despite filtering for over five days. Similarly, we were not able to emulate what described in section 3.3 and fabricate sonicated GO papers with the addition of borax cross-linker on the pre-formed GO papers because of the long filtration time. In the future, the sonication step will be further optimized by changing the sonication time and intensity.

4. Summary

We fabricated ultra-stiff and strong GO paper by directed-flow vacuum filtration using borax cross-linking, thermal annealing and sonication. A new fabrication method was developed where the GO suspension and borax solution are filtered separately, with the effect of enhancing the Young's modulus and strength of the resulting GO paper. Fig. 12a shows an overview of tensile modulus and ultimate strength for our GO paper, together with the properties for GO papers obtained from previous studies. Our GO paper provides strength in par with other proposed GO papers, and among the GO papers with the highest modulus. However many of these existing GO papers only come in the form of thin films, as making thicker films usually leads to less ordered microstructure and a decrease in modulus and strength. Therefore even though strength and modulus are high in some of these existing GO papers, their range of application is limited because restrictions in thickness limit their stiffness and the maximum forces they can sustain. Therefore we also report the ultimate force - axial stiffness chart Fig. 12b in order to take into account this limitation in thickness. The stiffest material we made (with a tensile modulus of 109.9 GPa and a flexural modulus of 45.7 GPa) is among the strongest and stiffest GO paper in the open literature.

This study also provides significant insights into the relationship between flexural and tensile properties of GO paper. The flexural modulus of GO paper is significantly lower than the tensile modulus, mainly because of micro-buckling and delamination during flexural deformation. GO paper should therefore be carefully selected depending on loading conditions if it is to carry tensile or flexural mechanical loads. The improved properties reported here,

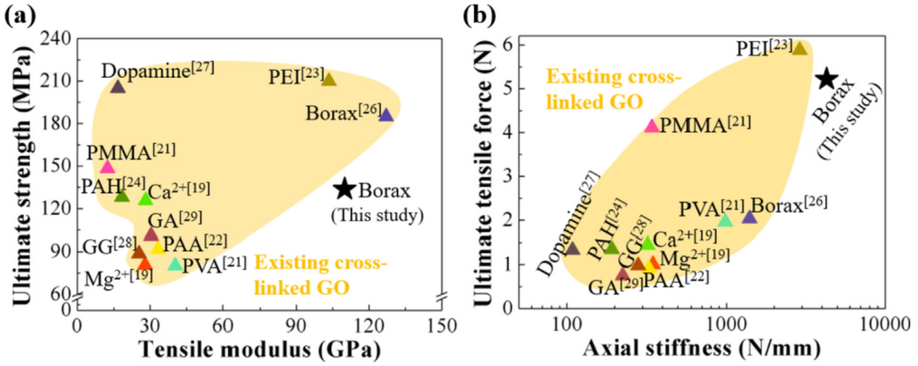

Fig. 12. Comparison of mechanical properties of GO paper fabricated with different cross-linkers: (a) tensile modulus and ultimate tensile strength; (b) axial stiffness and ultimate tensile force (a per unit length and width (1 mm) rectangular strip with different thicknesses). (A colour version of this figure can be viewed online.)

together with a relatively easy and scalable fabrication method, can expand the applications of GO paper including acoustic diaphragms, protective layers, supercapacitors or chemical filters.

Declaration of competing interest

The authors declare that they have no known competing financial interests or personal relationships that could have appeared to influence the work reported in this paper.

Acknowledgments

This study was supported by a Strategic Grant (STPGP 506395–17) from the Natural Sciences and Engineering Research Council of Canada. S.L. was partially supported by a McGill Engineering Doctoral Award.

References

[1] S.T. Woo, J. Han, J.H. Lee, S. Cho, K.W. Seong, M. Choi, et al., Realization of a high sensitivity microphone for a hearing aid using a graphene-PMMA laminated diaphragm, ACS Appl. Mater. Interfaces 9 (2) (2017) 1237–1246.

[2] Q. Zhou, J. Zheng, S. Onishi, M.F. Crommie, A.K. Zettl, Graphene electrostatic microphone and ultrasonic radio, Proc. Natl. Acad. Sci. 112 (29) (2015) 8942–8946.

[3] H. Tian, C. Li, M.A. Mohammad, Y.L. Cui, W.T. Mi, Y. Yang, Graphene earphones: entertainment for both humans and animals, ACS Nano 8 (6) (2014) 5883–5890.

[4] Y. Yao, X. Chen, H. Guo, Z. Wu, X. Li, Humidity sensing behaviors of graphene oxide-silicon bi-layer flexible structure, Sens. Actuators B Chem. 161 (1) (2012) 1053–1058.

[5] J. Scott Bunch, A.M. van der Zande, S.S. Verbridge, I.W. Frank, D.M. Tanenbaum, J.M. Parpial, et al., Electromechanical resonators from graphene sheets, Science 315 (5811) (2007) 490–493.

[6] R.K. Joshi, P. Carbone, F.C. Wang, V.G. Kravetsl, Y. Sul, I.V. Grigorieval, et al., Precise and ultrafast molecular sieving through graphene oxide membranes, Science 343 (6172) (2014) 752–754.

[7] J.H. Chu, L.B. Tong, M. Wen, Z.H. Jiang, K.S. Wang, H.J. Zhang, Graphene oxide film as a protective barrier for Mg alloy: worse or better is dependent on a chemical reduction process, Carbon 145 (2019) 389–400.

[8] U.A. Méndez-Romero, S.A. Pérez-García, X. Xu, E. Wang, L. Licea-Jiménez, Functionalized reduced graphene oxide with tunable band gap and good solubility in organic solvents, Carbon 146 (2019) 491–502.

[9] D.A. Dikin, S. Stankovich, E.J. Zimney, R.D. Piner, G.H. Dommett, G. Evmenenko, et al., Preparation and characterization of graphene oxide paper, Nature 448 (2007) 457–460.

[10] Y. Xu, H. Bai, G. Lu, C. Li, G. Shi, Flexible graphene films via the filtration of water-soluble noncovalent functionalized graphene sheets, J. Am. Chem. Soc. 130 (18) (2008) 5856–5867.

[11] X. Yang, J. Zhu, L. Qiu, D. Li, Bioinspired effective prevention of restacking in multilayered graphene films: towards the next generation of high-performance supercapacitors, Adv. Mater. 23 (25) (2011) 2833–2838.

[12] H.Y. Jeong, J.Y. Kim, J.W. Kim, J.O. Hwang, J. Kim, J.Y. Lee, et al., Graphene oxide thin films for flexible nonvolatile memory applications, Nano Lett. 10 (11) (2010) 4381–4386.

[13] V.H. Pham, T.V. Cuong, S.H. Hur, E.W. Shin, J.S. Kim, J.S. Chung, et al., Fast and simple fabrication of a large transparent chemically converted graphene film by spray-coating, Carbon 48 (7) (2010) 1945–1951.

[14] L.J. Cote, F. Kim, J. Huang, Langmuir-Blodgett assembly of graphite oxide single layers, J. Am. Chem. Soc. 131 (3) (2009) 1043–1049.

[15] C. Chen, Q.H. Yang, Y. Yang, W. Lv, Y. Wen, P.X. Hou, et al., Self-assembled free-standing graphite oxide membrane, Adv. Mater. 21 (2009) 3007–3011.

[16] J.W. Suk, R.D. Piner, J. An, R.S. Ruoff, Mechanical properties of monolayer graphene oxide, ACS Nano 4 (11) (2010) 6557–6564.

[17] J.T. Paci, T. Belytschko, G.C. Schatz, Computational studies of the structure, behavior upon heating, and mechanical poperties of graphite oxide, J. Phys. Chem. C 111 (49) (2007) 18099–18111.

[18] N.V. Medhekar, A. Ramasubramaniam, R.S. Ruoff, V.B. Shenoy, Hydrogen bond networks in graphene oxide composite paper: structure and mechanical properties, ACS Nano 4 (4) (2010) 2300–2306.

[19] S. Park, K.S. Lee, G. Bozoklu, W. Cai, S.T. Nguyen, R.S. Ruoff, Graphene oxide papers modified by divalent ions-enhancing mechanical properties via chemical cross-linking, ACS Nano 2 (3) (2008) 572–578.

[20] Y. Wang, Y. Mei, F. Huang, X. Yang, Y. Li, J. Li, et al., Ultra-robust and high-toughness graphene oxide papers via synergistic strengthening by addition of carbon-nanotubes and copper ions, Carbon 147 (2019) 490–500.

[21] K.W. Putz, O.C. Compton, M.J. Palmeri, S.T. Nguyen, L.C. Brinson, High-nano-filler-content graphene oxide-polymer nanocomposites via vacuum-assisted self-assembly, Adv. Funct. Mater. 20 (19) (2010) 3322–3329.

[22] S. Park, D.A. Dikin, S.T. Nguyen, R.S. Ruoff, Graphene oxide sheets chemically cross-linked by polyallylamine, J. Phys. Chem. C 113 (36) (2009) 15801–15804.

[23] Y. Tian, Y. Cao, Y. Wang, W. Yang, J. Feng, Realizing ultrahigh modulus and high strength of macroscopic graphene oxide papers through crosslinking of mussel-inspired polymers, Adv. Mater. 25 (21) (2013) 2980–2983.

[24] A. Satti, P. Larpent, Y. Gun'ko, Improvement of mechanical properties of graphene oxide/poly(allylamine) composites by chemical crosslinking, Carbon 48 (12) (2010) 3376–3381.

[25] Q. Cheng, M. Wu, M. Li, L. Jiang, Z. Tang, Ultratough artificial nacre based on conjugated cross-linked graphene oxide, Angew Chem. Int. Ed. Engl. 52 (13) (2013) 3750–3755.

[26] Z. An, O.C. Compton, K.W. Putz, L.C. Brinson, S.T. Nguyen, Bio-inspired borate cross-linking in ultra-stiff graphene oxide thin films, Adv. Mater. 23 (33) (2011) 3842–3846.

[27] W. Cui, M. Li, J. Liu, B. Wang, C. Zhang, L. Jiang, et al., A strong integrated strength and toughness artificial nacre based on dopamine cross-linked graphene oxide, ACS Nano 8 (9) (2014) 9511–9517.

[28] D. Kang, Z. Cai, Q. Jin, H. Zhang, Bio-inspired composite films with integrative properties based on the self-assembly of gellan gum-graphene oxide cross-linked nanohybrid building blocks, Carbon 91 (2015) 445–457.

[29] Y. Gao, L.Q. Liu, S.Z. Zu, K. Peng, D. Zhou, B.H. Han, et al., The effect of interlayer adhesion on the mechanical behaviors of macroscopic graphene oxide papers, ACS Nano 5 (3) (2011) 2134–2141.

[30] K. Hu, M.K. Gupta, D.D. Kulkarni, V.V. Tsukruk, Ultra-robust graphene oxide-silk fibroin nanocomposite membranes, Adv. Mater. 25 (16) (2013) 2301–2307.

[31] T. Gong, D.V. Lam, R. Liu, S. Won, Y. Hwangbo, S. Kwon, et al., Thickness dependence of the mechanical properties of free-standing graphene oxide papers, Adv. Funct. Mater. 25 (24) (2015) 3756–3763.

[32] R.A. Soler-Crespo, W. Gao, L. Mao, H.T. Nguyen, M.R. Roenbeck, J.T. Paci, et al., The role of water in mediating interfacial adhesion and shear strength in graphene oxide, ACS Nano 12 (6) (2018) 6089–6099.

[33] K. Hu, X. Xie, T. Szkopek, M. Cerruti, Understanding hydrothermally reduced graphene oxide hydrogels: from reaction products to hydrogel properties, Chem. Mater. 28 (6) (2016) 1756–1768.

[34] H.P. Mungse, O.P. Sharma, H. Sugimura, O.P. Khatri, Hydrothermal deoxygenation of graphene oxide in sub-and supercritical water, RSC Adv. 4 (2014) 22589–22595.

[35] P. Wambua, J. Ivens, I. Verpoest, Natural fibres: can they replace glass in fibre reinforced plastics? Compos. Sci. Technol. 63 (9) (2003) 1259–1264.

[36] T. Taniguchi, S. Kurihara, H. Tateishi, K. Hatakeyama, M. Koinuma, H. Yokoi, et al., pH-driven, reversible epoxy ring opening/closing in graphene oxide, Carbon 84 (2015) 560–566.

[37] O.C. Compton, S.T. Nguyen, Graphene oxide, highly reduced graphene oxide, and graphene: versatile building blocks for carbon-based materials, Small 6 (8) (2010) 711–723.

[38] Y. Qiu, F. Collin, R.H. Hurt, I. Külaots, Thermochemistry and kinetics of graphite oxide exothermic decomposition for safety in large-scale storage and processing, Carbon 96 (2016) 20–28.

[39] K.S. Andrikopoulos, G. Bounos, D. Tasis, L. Sygellou, V. Drakopoulos, G.A. Voyiatzis, The effect of thermal reduction on the water vapor permeation in graphene oxide membranes, Adv. Mater. Interfaces 1 (8) (2014), 1400250.